AD-A192 356 COMPUTER PROGRAMS FOR HIGH-CURRENT BEAM TRANSPORT IN ACCELERATORS(U) MISSION RESEARCH CORP ALBUQUERQUE NM B B GODFREY DEC 87 AMRC-R-1012 N60921-85-C-0044 1/1

UNCLASSIFIED F/G 20/7 NL

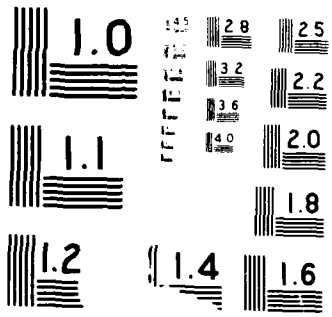
1.0
1.1
1.2
1.4
1.6
1.8
2.0
2.2
2.5
2.8
3.2
3.6
4.0

AMRC-R-1012
Copy 115

Mission Research Corporation

COMPUTER PROGRAMS FOR HIGH-CURRENT BEAM TRANSPORT IN ACCELERATORS

Brendan B. Godfrey

December 1987

Sponsored by: Defense Advanced Research Projects Agency

Monitored by Naval Surface Weapons Center
under Contract N60921-85-C-0044 to SAIC

Science Applications International Corporation,
Subcontract 15-860022-79

Prepared by: MISSION RESEARCH CORPORATION
1720 Randolph Road, SE.
Albuquerque, NM 87106-4245

Computer programs for high-current beam transport in accelerators

Brendan B. Godfrey
Mission Research Corporation, Albuquerque, NM 87106, USA

Numerical techniques exist for modeling particle beam dynamics in high current accelerators at several levels of fidelity. Equilibria can be determined with beam envelope codes, particle ray-tracing, Vlasov equilibrium solvers, and single-disk particle codes. The linear stability of these equilibria is addressed with dispersion relations solved numerically, linearized PIC codes, and single- and multi-component beam centroid programs. Beam nonlinear dynamics are investigated with multidimensional PIC codes employing either the complete electromagnetic field equations or various approximations to them. Each of these options is discussed, and several examples are provided.

I. INTRODUCTION

A. Accelerator Types

Historically, high energy particle accelerators were developed as research tools for nuclear and high energy physics research. These accelerators were low current devices for which the beam dynamics could be modeled computationally with a small number of noninteracting particles. Spacecharge, wakefield, and other corrections were added to the calculations as the currents of interest gradually increased. Several sophisticated yet reasonably fast-running computer programs now exist for modest current, high energy accelerators; they are described in the chapter by R. Cooper.

Since the 1960's high current, moderate energy, pulsed-diode electron accelerators have been built, principally for materials research and flash radiography. More recently, similar techniques have been used to create intense light ion beams for fusion purposes. Self-consistently treating beam-generated fields is critical for accurate numerical simulation of high current diodes, and even the earliest steady-state codes included first-principles calculations of electrostatic and azimuthal magnetic fields. Time-dependent diode codes, borrowed from plasma physics, also include self-fields in an integral manner. The chapter by J. Quintenz and D. Seidel provides details.

High current, high energy induction accelerators first were studied in the late 1960's as injectors for electron ring accelerators.[1] (Research on betatrons, of course, goes back much further.[2,3]) More recently, renewed investigations have been motivated by heavy ion fusion, free electron lasers, and other applications. Treating induction accelerators numerically is challenging due to the large range of temporal and spatial scales involved. Simultaneously, self-field effects must be included, especially for low energy sections. A wide variety of computational tools, from simple envelope models to multidimensional particle-in-cell (PIC) simulations, have been developed and are reviewed in this chapter.

Several collective-effect concepts have been proposed to utilize the very large fields which can, in principle, exist in plasmas to accelerate electrons or ions. Collective ion acceleration,[4,5] laser beatwave acceleration,[6,7] and plasma wakefield acceleration[8] are examples. Typically, PIC codes are used to explore these ideas numerically.

B. High Power Induction Accelerators

A linear induction accelerator achieves high particle energies by applying moderate voltages at successive acceleration gaps only while the beam is passing. The gaps are driven by ferrite cores or dielectric lines, which are in turn energized by conventional pulse power sources. Figure 1 illustrates schematically a portion of the beam line of a ferrite-loaded accelerator. Pavlovskii and

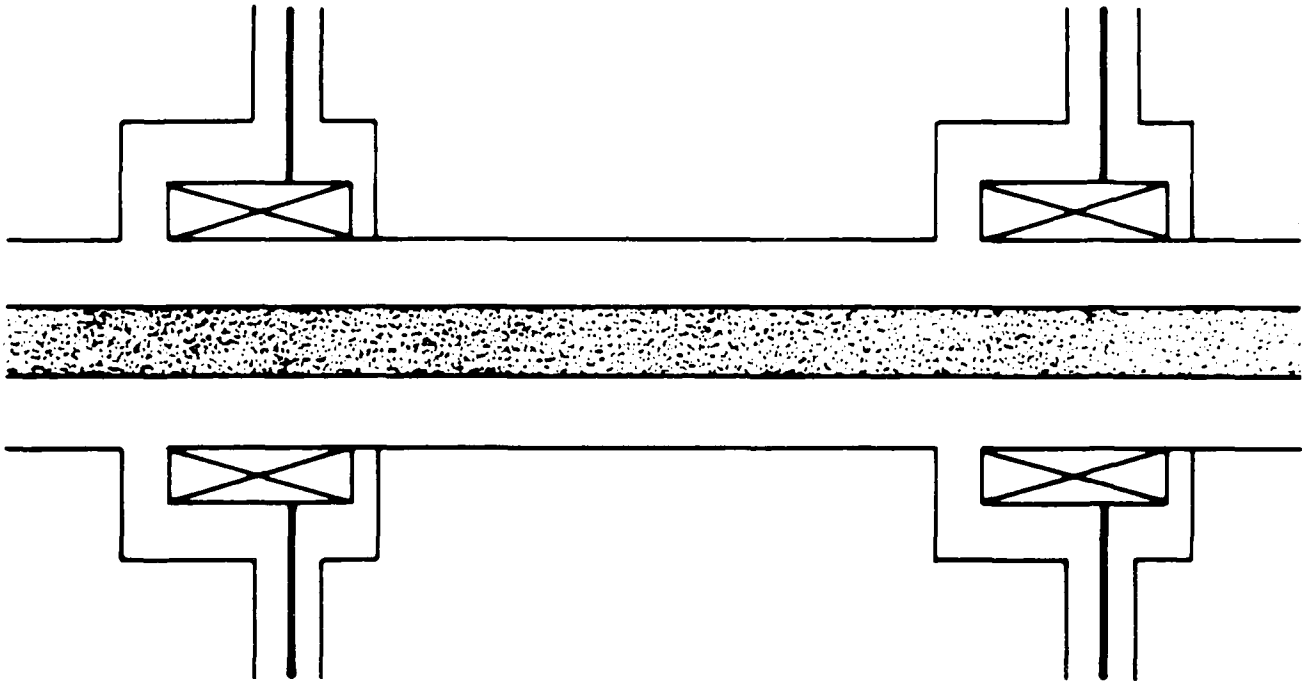

FIG. 1. Simplified representation of induction accelerator beam line, showing two ferrite core modules. Solenoidal magnetic field coils typically are placed between gaps.

co-workers published extensively on linear induction accelerators during the 1970's.[9] Two half-terawatt electron accelerators are in operation, the 10 kA, 42 MeV, ferrite core ATA at Lawrence Livermore National Laboratory[10] and the 30 kA, 16 MeV dielectric line RADLAC at Sandia National Laboratories.[11]

The acceleration gaps can perturb the beam in several ways. Radial electric fringe fields may cause radial oscillations,[12] while the interrupted magnetic image current may trigger transverse displacements.[13] The beam breakup instability, associated with TM_{1n0} gap modes, produces particularly dangerous transverse oscillations.[14,15] Even in the absence of gaps, the diocotron instability is disruptive for low energy annular beams.[16] The resistive wall instability is unimportant, however.[17]

Various recirculation schemes are being considered to reduce the size, weight, and cost of induction accelerators.[18,19] Figure 2 depicts a basic design. An electron beam is injected through

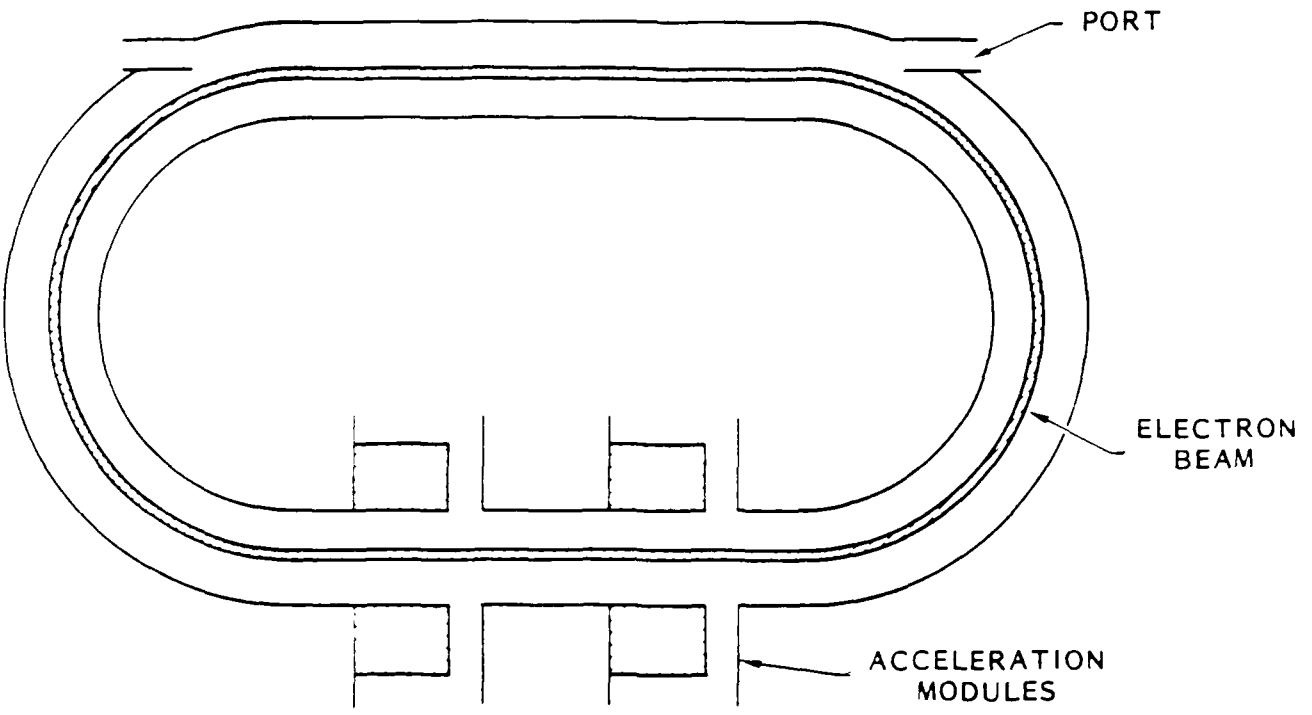

FIG. 2. Schematic representation of a racetrack induction accelerator.

an entrance port, passes several times through the acceleration modules, and is extracted through the exit port. Because injection and extraction with minimal beam loss is difficult even conceptually, some designs employ an open helix rather than a closed racetrack geometry.[20] Bending magnetic fields in the curved sections must be ramped up rapidly to keep the beam in the drift tube. Periodic strong-focusing fields in the bends is sometimes proposed to increase the energy bandwidth there.[21] The betatron also is a recirculating induction accelerator, although without discrete gaps. A slowly increasing vertical magnetic both guides and accelerates the beam.[22] In addition, a toroidal magnetic field, perhaps augmented by periodic strong focusing, is needed to confine high currents at low to moderate energies.[23] Injection and extraction remain problems.[24,25]

Beam line curvature introduces the negative mass instability,[26,27] which can destroy a recirculating beam on the μsec time scale. Figure 3 shows the typical saturated state of a long wavelength negative mass mode in a high current betatron.[28] The instability arises because higher energy beam particles in a bend move to larger radii and consequently fall back in the beam relative to lower energy particles. Particle clumps grow spontaneously, as if like particles attracted. Periodic strong focusing, mentioned above, slows the negative mass instability but triggers a parametric three-wave instability similar to the Raman instability of the free electron laser.[29] Its growth rate can be very large. Single particle resonances also are potentially serious in recirculating accelerators, so special care must be taken to avoid magnetic field errors.[30]

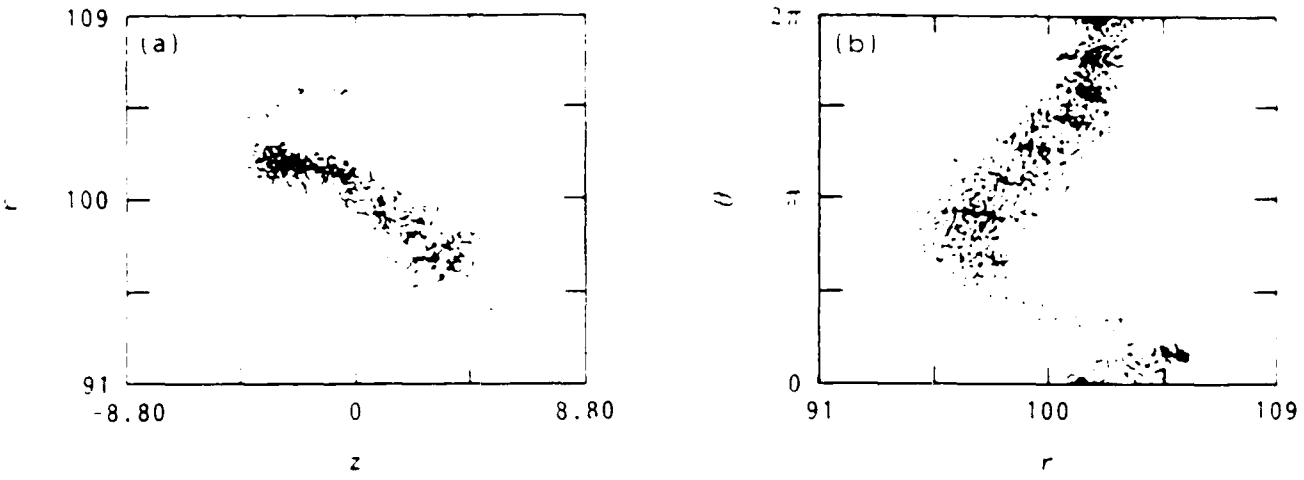

FIG. 3. The (a) z-r and (b) r-θ cross sections of a 10 kA, 5 MeV electron beam in a 1 m radius betatron 260 nsec after the onset of a long wavelength negative mass instability; B_θ = 1 kG.

Ion-focused transport (IFT) in induction electron accelerators, either separately or in conjunction with magnetic transport, has certain desirable features[31]: magnetic focusing elements are unnecessary, the beam breakup instability is suppressed,[32] and the energy bandwidth of magnetic bending elements is increased. Injection and extraction for racetrack geometries remain problems, although more possible solutions exist.[33] Low density ionized channels can be created by lasers, low energy electron beams, or electrical discharges. In an experiment at Sandia National Laboratories, a 10 m ion channel was produced with a 1 A, 500 V electron beam, and a 15 kA, 1 MeV electron beam guided by the channel through three 90° bends.[34] The most serious potential difficulty for IFT is the ion resonance instability.[35,36] It can, at a minimum, be postponed by using heavy ions, like Xenon.

Experiments on the PULSELAC device have demonstrated that electron neutralization in ion accelerators also is effective.[37] Extensive reviews of high current induction accelerators can be found in the proceedings of a recent NATO Advanced Study Institute.[38]

C. Numerical Models

Beam dynamics in induction and other high-current accelerators can be treated numerically in a variety of approximations. Beam equilibria often are computed economically with envelope codes. Steady-state particle ray-tracing codes are useful in modeling diodes and short transport sections. If the beam particle equilibrium distribution is approximately known (in terms of constants of motion), then the beam current and field radial profiles are easily determined numerically. Finally, radially-resolved single disk 'C codes are used to obtain the evolution of the beam equilibrium when beam properties vary slowly through the pulse.

Beam stability properties in an accelerator can be determined simply by solving numerically an analytical linear dispersion relation, if it is known. Alternatively, linearized PIC codes are

fairly efficient at providing the growth rates and field structure of three-dimensional instabilities for specified one-dimensional (typically, radially-resolved) equilibria. These two procedures yield instability growth rates at fixed points in the accelerator. The linear development of transverse oscillations due to, for instance, the beam breakup instability as the beam travels through the entire accelerator can be modeled efficiently by treating the beam as a string of rigid disks, and the gap fields as lumped circuit elements. (Early stages of the negative mass instability have been handled in the same way as well.) Beam thermal effects sometimes can be introduced by representing the beam by multiple sets of interlaced disks. If required, the disk radii can evolve according to the envelope equations mentioned above.

At some point, adding more and more physics to simple numerical models becomes unproductive, and PIC codes should be used instead. This is particularly true, if the nonlinear evolution of instabilities is important. Though expensive to employ, PIC codes describe the interaction of beam particles with applied and self-consistent electromagnetic fields in microscopic detail. Typically, PIC accelerator simulations are performed in two-dimensional r-z geometry, although three-dimensional calculations sometimes are necessary. Single disk PIC codes resolved in r-θ can be used to investigate long wavelength transverse instabilities. When electromagnetic waves are unimportant, employing the Darwin field approximation saves some time. The frozen field approximation could be applied to plasma wakefield calculations.

II. EQUILIBRIUM AND QUASI-EQUILIBRIUM COMPUTATIONS

A. Beam Envelope Codes

In most cases $\nu/\gamma \ll 1$ for relativistic electron beams in accelerators, although not necessarily in diodes. (ν is the beam current normalized to 17 kA, $\gamma = (1-V^2)^{-1/2}$ is the particle relativistic energy normalized to its rest mass, and V is the particle velocity normalized to the speed of light.) As a result $V_r \ll V_z$, and the paraxial approximation that changes in V_r do not cause changes in V_z can be invoked. Applying the virial theorem to the beam transverse dynamics then yields a simple differential equation for the beam rms radius, R.[39]

$$\frac{d}{dt}\gamma\frac{d}{dt}R = \frac{\epsilon^2 + P_\theta^2}{\gamma R^3} - \frac{\omega_c^2 R}{4\gamma} - \frac{\gamma U}{R} - F_r \tag{1}$$

Auxiliary quantities are the normalized emittance ϵ,

$$\epsilon^2 = \gamma^2(r^2V_r^2 - \ldots), \tag{2}$$

and the self-field function U,

$$U = (E_r - VB_\theta)/V\gamma r) \approx \nu\frac{\nu}{\gamma}\left[1 - \frac{1-f}{\nu^2}\right] \tag{3}$$

P_θ is the particle angular momentum normalized to mc, $\omega_c = qB_z/mc$ is its gyrofrequency, F_r is any applied radial acceleration, and f is the charge neutralization fraction provided by a

background plasma. Current neutralization could be incorporated in Eq. (3) as well. Note that Eq. (1) reduces to the single particle radial equation of motion for ϵ small.

Equation (1) as it stands is dissipationless, and the normalized emittance is assumed constant. In reality, single particle scattering causes a slow growth in emittance,[40] as do weak instabilities. In addition, phase-mix damping due to a spread in single particle oscillation frequencies leads to a gradual decrease in d^2R/dt^2 with a corresponding increase in ϵ.[41] These corrections usually can be ignored in accelerator calculations.

One of many problems to which Eq. (1) has been applied is the chopping of the initially continuous beam in the PHERMEX standing-wave RF accelerator at Los Alamos National Laboratory.[42] The effects of apertures and RF focusing fields as well as RF accelerating fields are included. Despite the simplicity of the model, agreement between code predictions and experimental measurements is good. Figure 4 illustrates typical output for an individual micropulse out of a sequence of several. Calculations take less than a minute on a minicomputer.

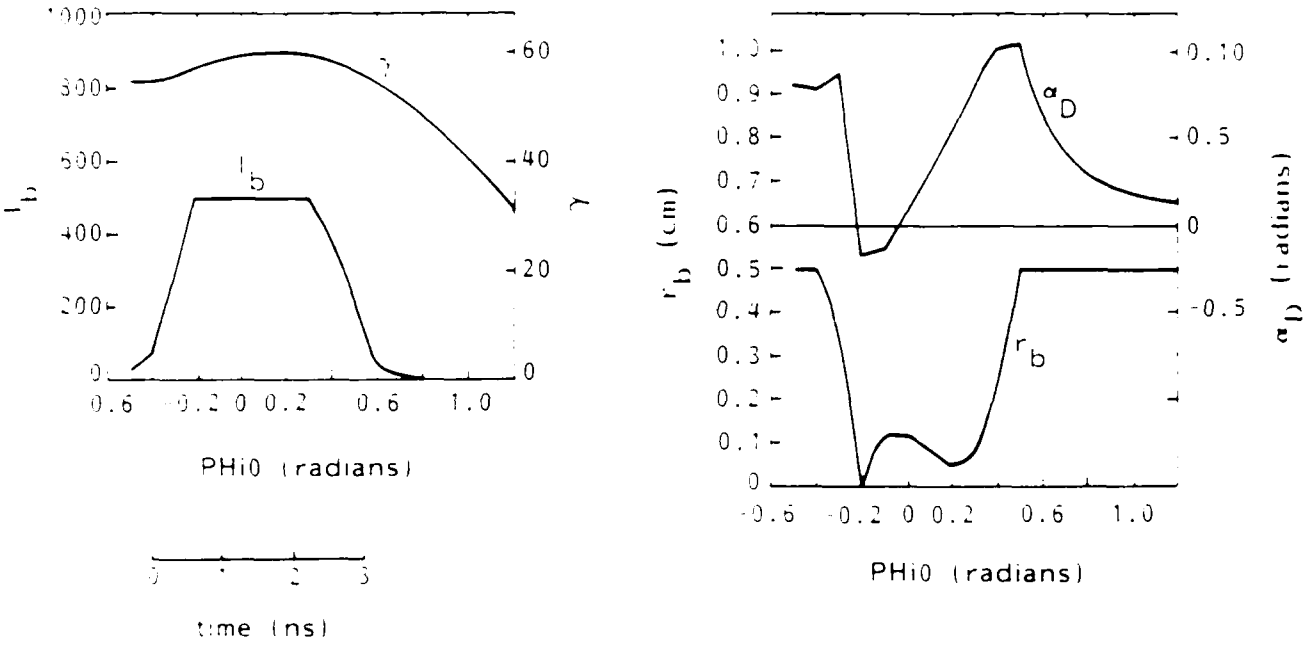

FIG. 4. PHERMEX beam current (I_b), energy (γ), radius (r_b), and divergence (α_D) versus RF phase as predicted by XLR8R code.

The envelope model also can be used to represent one particle species in a multispecies hybrid model. For instance, the SEE code at Lawrence Livermore National Laboratory, which is used to investigate secondary electron expulsion from an IFT channel, describes the electron beam with an envelope equation and the channel electrons with discrete particles.[43]

B. Steady-State Ray-Tracing Codes

Long-puise electron and ion diodes are treated efficiently by ray-tracing codes with applied and self-consistent fields.[44,45] These codes also can be used for steady-state beam transport in

accelerator segments. At each iteration a few hundred beam particles are transported along their entire trajectories on the computational mesh using fields determined on the previous iteration, and their charge and current contributions accumulated. The static beam fields then are recomputed from the charge and current distributions. This process is repeated a few dozen times until convergence is achieved. Only about a minute of CRAY-1 computer time is needed. Often the output is used to initialize other computer programs.[46] Particle ray-tracing codes are described more fully in the chapter by J. Quintenz and D. Seidel.

C. Kinetic Equilibrium Codes

Any cylindrically symmetric beam equilibrium can be expressed as a distribution function $F(H, P_z, P_\theta)$ of the particle energy and canonical axial and angular momenta.[47]

$$H = \gamma - \phi(r) \tag{4}$$

$$P_z = p_z - A_z(r) \tag{5}$$

$$P_\theta = r[p_\theta - A_\theta(r)] \tag{6}$$

All the beam properties can be determined from F. The scaler and vector potentials appearing in Eqs. (4)–(6) are given in terms of the beam charge and current densities by the usual expressions,

$$\frac{1}{r}\frac{d}{dr}r\frac{d}{dr}\phi = -4\pi\rho \tag{7}$$

$$\frac{1}{r}\frac{d}{dr}r\frac{d}{dr}A_z = -4\pi J_z \tag{8}$$

$$\frac{d}{dr}\frac{1}{r}\frac{d}{dr}rA_\theta = -4\pi J_\theta \tag{9}$$

The charge and current densities are, in turn, given by integrals over the distribution function.

$$\rho = \int F d^3p \tag{10}$$

$$J_z = \int V_z F d^3p \tag{11}$$

$$J_\theta = \int V_\theta F d^3p \tag{12}$$

Usually, it is more convenient to perform the integrals over the constants of motion instead of the kinetic momenta. The Jacobian of the transformation is γ / rp_r. Care must be taken in evaluating the integrals near radial turning points, where $p_r = 0$.

In the absence of instabilities, reasonable guesses can be made for the particle distribution function in an induction accelerator. Since canonical angular momentum is conserved, the P_θ distribution is determined by injector properties. For a shielded injector (i.e., $B_z^c = 0$), $P_\theta = 0$ and F is proportional to $\delta(P_\theta)$. More generally, the P_θ distribution is estimated by solving $rA_\theta(r) = P_\theta$ for r at the cathode and then substituting for r in $n^c(r)/rB_z^c$ at the cathode. The H distribution is obtained with equal ease: H is approximately constant for all particles at the injector and increases by a constant amount at each gap. Finally, the spread in P_z is determined by the angular scatter in the beam particles, which is small. One plausible expression is $\exp(P_z T)$, where $T = p_0 \cdot p_\perp^2 \; p_z^2) \; 2$ is proportional to the Bennett temperature.[48,49] (T can be made a function of P_θ, if a strong correlation exists between the particle scatter angle and radius.) In all, we have an expression of the sort

$$F(H, P_z, P_\theta) = C\delta(H - H_0)\exp(P_z/T)\{n/rB_z\}\left((rA_\theta)^{-1}(P_\theta)\right) \tag{13}$$

Equations (4)–(12) are easily solved numerically. Density profiles obtained from the computer program ORBIT for four simple beam distribution functions are shown in Fig. 5.[50] Convergence

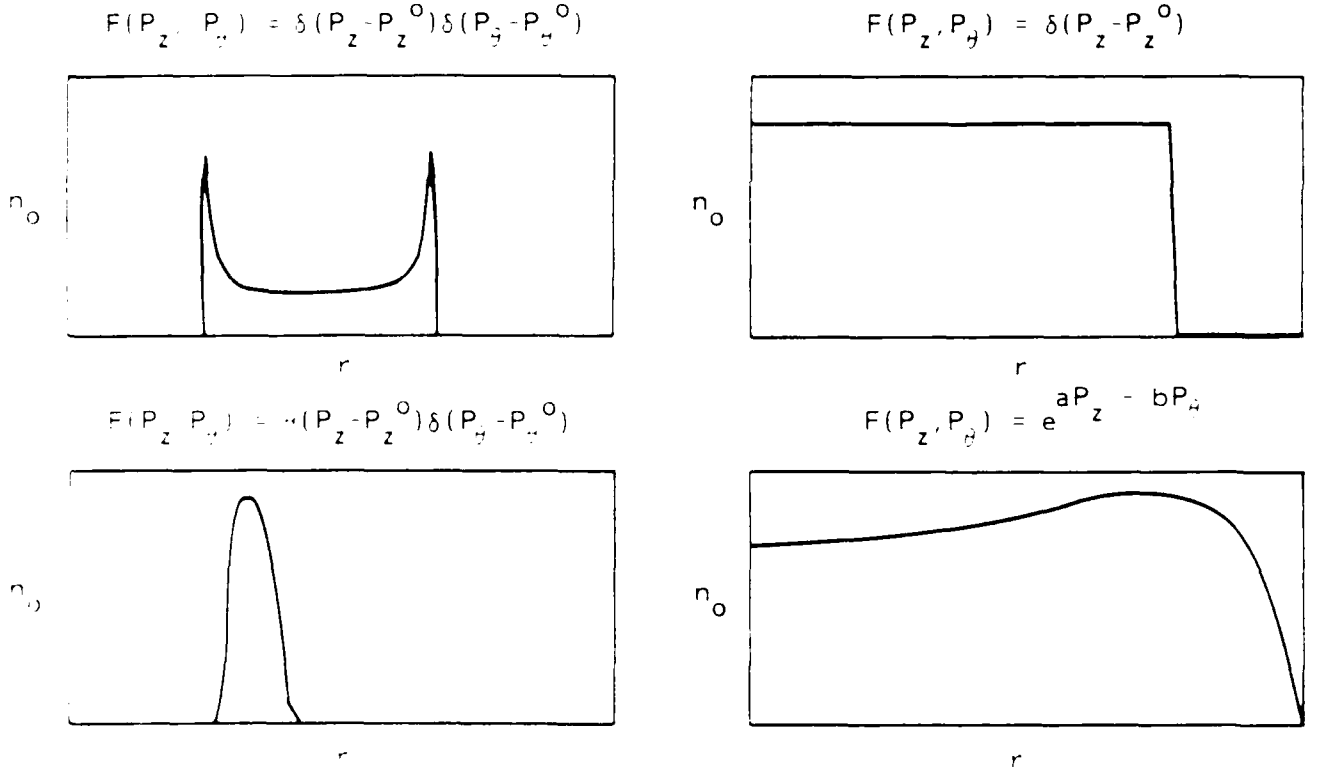

FIG. 5. Sample density profiles for monoenergetic beams, obtained by solving Eqs. (4)–(12) with the indicated distribution functions.

is achieved in about ten iterations, which can be done in a few seconds on a CRAY-1 computer. Equilibria obtained in this way have been used to initialize some of the linear and nonlinear PIC

codes discussed later. Incidentally, the distribution $C \cdot \delta(H - H_0) \cdot \exp(P_z\ T)$ is a nonparaxial generalization of the Bennett distribution.

ORBIT has been employed in magnetically insulated ion diodes as well. Finite temperature effects, gas prefill, and electron injection with nonzero energy were investigated, and both axial and azimuthal applied magnetic fields were considered.[51] Using ORBIT eliminated the need for many of the assumptions and approximations necessary in the analytic treatment of magnetic insulation.

D. Single Disk Particle Codes

The particle constants of motion are changed, if an abrupt transition occurs in the external focusing fields; a dynamic calculation is necessary to obtain the new beam equilibrium. This is particularly simple in the case of relativistic beams, for which the effects of the transverse self-fields (e.g., E_r and B_θ) nearly cancel. The beam then is represented as a single disk of a few hundred noninteracting particles subject only to the applied fields. Such codes can be very fast, even for transport over long distances. (Single disk particle codes in which transverse self-fields are retained are, in fact, PIC codes, discussed in a subsequent section.)

The WIRE code at Lawrence Livermore National Laboratory is a good example.[52] It is used routinely to compute ETA and ATA beam transport in various focusing systems. (The ETA accelerator, now disassembled, was a 8 kA, 5 MeV prototype for ATA.) Among the elements considered are solenoidal magnetic lenses, ion channels, grounded wires centered on the axis, and metal foils. For the centered conducting wire the radial electric field is fixed by demanding that the potential between the wire and the drift tube be zero, which requires a simple integration over the disk density profile. Fields associated with focusing foils were derived by Adler.[53] A typical 1280 particle run with numerous focusing elements over 600 cm takes about 30 sec on a CRAY-1 computer.

DISC, a similar program at Sandia National Laboratories, has been used to optimize matching of the RADLAC beam onto an IFT channel.[54] The experimental configuration modeled is shown in Fig. 6. A 20 kA, 16 MeV, annular electron beam enters from the left in vacuum along a 17 kG axial magnetic field. The beam was born at an immersed cathode and so has significant canonical angular momentum; it is in the slow mode of rotation. The beam then enters a region of rapidly decreasing magnetic field, where it spins up and begins to expand. The expansion is arrested by a pair of focusing foils, and the beam finally is captured by the IFT channel at the right.

Figure 7 is a sequence of three particle plots illustrating the evolution of an initially off-center beam. Little of the beam current is lost at the transition despite the large initial offset. Moreover, the beam is centered by the IFT channel within 100 cm of transport, although its emittance increases substantially. DISC computations such as this consume only a few minutes of minicomputer time.

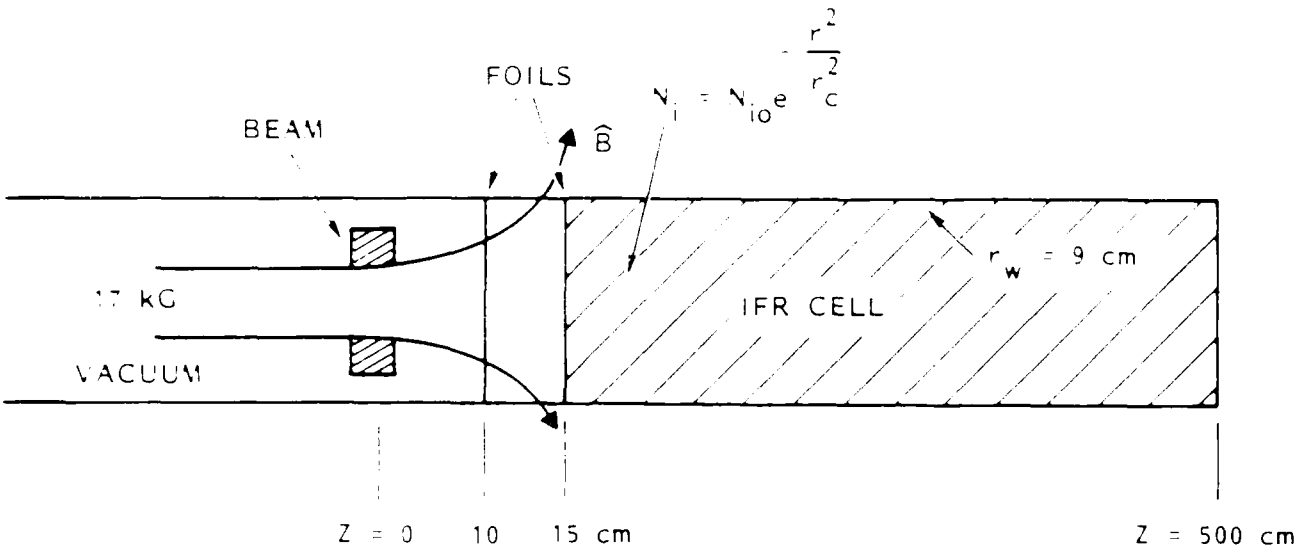

FIG. 6. Experimental geometry for DISC code simulation of RADLAC beam extraction from magnetic guide field and capture by IFT channel.

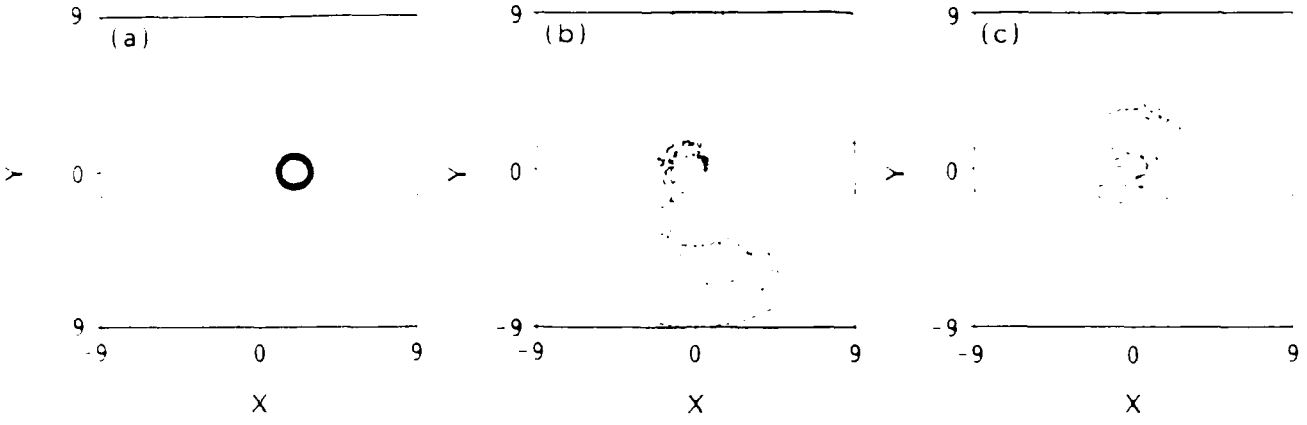

FIG. 7. Cross sections of an initially offset RADLAC beam at (a) 0 cm, (b) 40 cm, and (c) 100 cm after extraction from a 17 kG guide field into an IFT channel, computed by the DISC code for the geometry depicted in Fig. 5. The outer dashed circle is the drift tube, and the inner is the beam RMS radius relative to the drift tube axis.

Similar single disk codes have been employed to study electron beam expansion in air due to scattering.[55] The Moliere[56] or Keil-Zeitler-Zinn[57] formalism should be utilized, depending on whether many or few scattering events occur in a betatron wavelength.

III. LINEAR STABILITY COMPUTATIONS

A. Dispersion Relation Codes

If the beam equilibrium is not too complicated, it usually is possible to describe the growth of linearly unstable modes by a dispersion relation $F(\omega, \underline{k}, \alpha)$, where ω is the (complex) mode frequency, $\underline{k}$ is its wavenumber, and α the set of parameters describing the beam and accelerator. Peak growth rates of absolute instabilities are obtained as $Im(\omega)$ for the zeroes of F, maximized over $\underline{k}$.[58] Peak spatial growth rates of convective instabilities sometimes are given by the temporal growth rates divided by the corresponding group velocities, $\partial\omega/\partial k$, again maximized over $\underline{k}$. More often, a saddle point analysis is required. The convective growth of the resistive wall instability in an induction accelerator can be derived by this method, for instance.[59]

Complex zeroes of locally analytic functions are easily obtained iteratively by Muller's method.[60] In essence, the algorithm fits a quadratic curve to three values of the function and then employs the curve to estimate the location of a zero. At each iteration the function is evaluated at the estimated zero from the preceding cycle, and a new estimate made based on this and the two preceding function evaluations. A zero typically can be determined to a relative accuracy of 10^{-5} by this method in six to ten cycles. Subroutines implementing Muller's method are widely available, one can be obtained from the author.[61]

Although Muller's method can be applied to polynomial functions, the Vieta formula solved by the Newton-Raphson method is more efficient.[62] Moreover, it gives all the zeroes simultaneously. Many implementations are available, some accommodating repeated zeroes.[63] There are, of course, many more techniques for finding zeroes of functions than the two mentioned here.

The dispersion function need not be known analytically to apply Muller's method, if it can be computed numerically with sufficient accuracy. An example is the GRADR code, which determines the normal modes of cylindrically symmetric, radially inhomogeneous, particle beams in the laminar flow approximation.[64] The cylindrical equilibrium is evaluated from six nonlinear, coupled, algebraic and first-order differential equations. Four follow from Maxwell's equations plus the fluid equations, while two can be specified arbitrarily to select a desired equilibrium.[65] The two constraint equations should, of course, be physically realizable. One constraint almost always is appropriate: total particle energy, kinetic plus potential, must be constant across the beam and equal to the injection energy. As a second constraint, typically we let the current density profile of the beam be specified at injection. Conservation of canonical angular momentum then determines the current density profile within the accelerator drift tube. The resulting system of equations is solved iteratively. Convergence is achieved after a few dozen cycles, unless the beam is very near the space charge limit.

Given an equilibrium determined in this or any other way, GRADR then solves the corresponding linearized equations to obtain eigenmodes and eigenvalues. The linear equations form a fourth-order Sturm-Liouville system in radius. The equations are integrated twice from the axis to the outer wall with distinct arbitrary choices for the eigenfunction values at the axis, subject to the two boundary conditions there. A Fehlberg fourth-fifth-order Runge-Kutta routine[66] is employed. Arbitrary linear combinations of the two solutions then are used to evaluate the two boundary conditions at the wall, and the determinant for the unknown coefficients serves as the dispersion function to which Muller's method is applied. Solutions can be obtained at the rate of one per second on a CRAY-1 computer.

GRADR was used extensively in designing the RADLAC accelerator.[67] Typical frequencies and growth rates for the resistive wall instability are shown in Fig. 8. Note the existence of

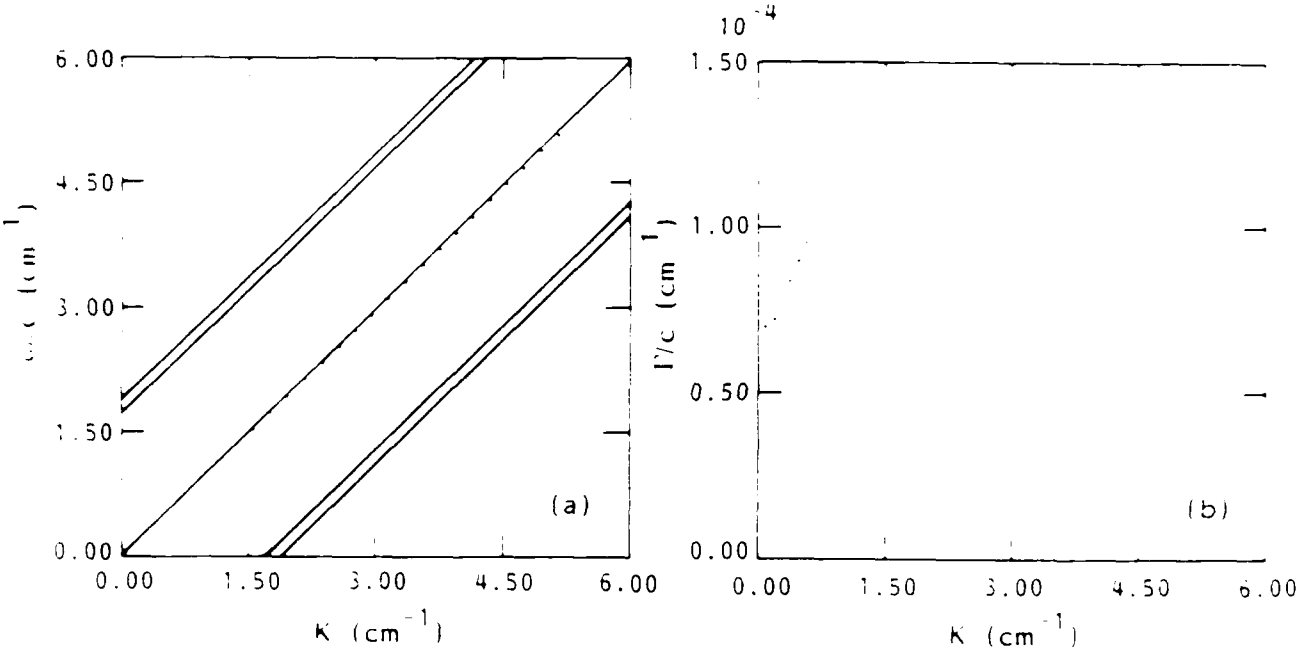

FIG. 8. Predicted (a) frequencies and (b) growth rates of the $m = 1$ transverse resistive wall instability of a 100 kA, 25 MeV annular electron beam propagating along a 20 kG guide field in a 2.5 cm radius stainless steel drift tube. Straight lines in (a) are the edges of cyclotron and space charge resonance bands due to the variation of beam parameters with radius.

branch points (straight lines in Fig. 8(a)) due to radial inhomogeneity in the beam density. High accuracy must be demanded of the differential equation solver when zeroes lie near branch points, as is the case here.

GRADR originally was written to investigate collective ion acceleration. In many collective acceleration concepts the wave phase velocity is controlled by adiabatically varying some external parameter α, such as the guide field strength[68] or the drift tube radius.[69] The corresponding

change in wave amplitude can be calculated from conservation of wave energy, which is an option in the code.[7]

B. Linearized PIC Codes

The stability of more complicated equilibria, particularly those in which kinetic effects are important, can be established with linearized PIC codes. In such models equilibrium fields and particle orbits are obtained from nonlinear PIC codes or by other means (e.g., the ORBIT code, discussed earlier). Then, perturbations to the equilibrium orbits due to wave fields are accumulated along the unperturbed orbits and used as source terms for the wave fields themselves. This leap-frog procedure in time is similar to that of standard PIC codes.

The linearized particle equations of motion are much more complicated than their nonlinear counterparts, however.[71] Formally,

$$P_1 = E_1 - V_1 \times B_1 - V_1 \times B_0 - X_1 \cdot \delta (E_0 - V_0 \times B_0) \quad \delta X \tag{14}$$

$$V_1 = P_1 \gamma_0 - P_1 \cdot P_0 \; P_0 \gamma_0^3 \tag{15}$$

$$\dot{X}_1 = V_1 \tag{16}$$

A savings is achieved, therefore, only if significantly fewer particles are needed, and the effective dimensionality of the problem is reduced.

The linearized PIC code KMRAD, for example, realizes both of these savings.[72] Cylindrically symmetric, possibly slowly evolving, beam equilibria are determined by a one-dimensional, radially resolved, nonlinear PIC code embedded in KMRAD. Three-dimensional linearized quantities also are resolved radially on a spatial mesh but are Fourier decomposed in z and θ; one (k_z, m) mode is treated at a time. The instability growth rate of the fastest unstable wave with the selected mode numbers is determined from the exponential growth of field energy in the simulation. Field and current radial profiles also are available. Thus, KMRAD simulates three-dimensional linearized dynamics but requires computer resources comparable to those of a one-dimensional code. Of order 1000 particles are followed. Answers are obtained with one to two minutes of CRAY-1 computer time.

KMRAD was employed recently to predict two-stream instability growth rates in IFT channels for recirculating accelerators.[73] A comparison between KMRAD kinetic and cold-beam analytical results for a channel over-dense by a factor of two is in Fig. 9. Agreement with growth rates from the IVORY three-dimensional PIC code, described later, is good. In under-dense channels the electron-electron instability is replaced by a much slower electron-ion instability. The code also has been exercised on resistive instabilities in much higher density channels.

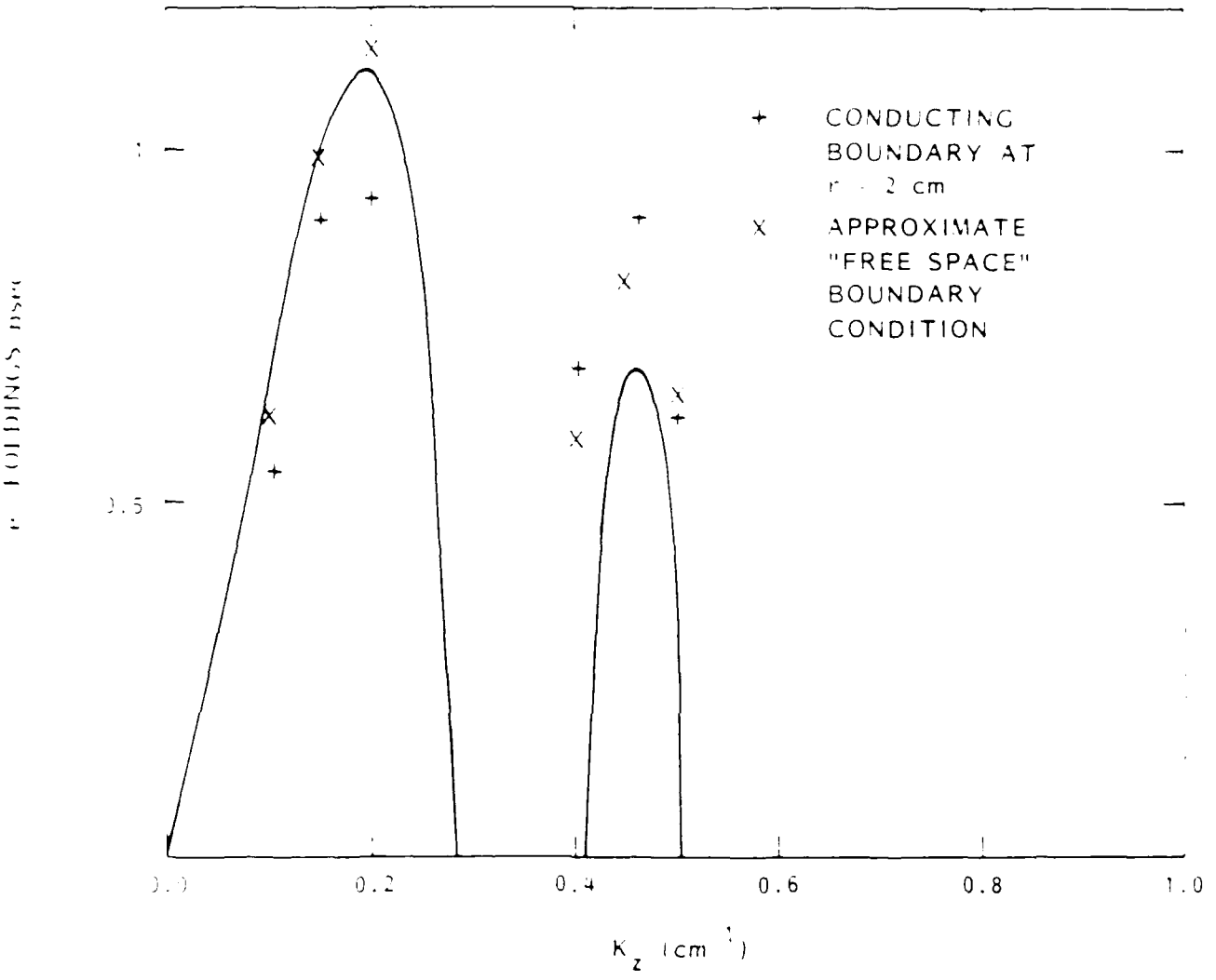

FIG. 9. Growth rates of the $m = 1$ two-stream instability between a 450 A, 35 MeV, 0.25 cm radius electron beam and electrons of an 1 cm radius IFT channel with line density initially twice that of the beam.

C. Single-Component Beam Centroid Codes

The previous two subsections described methods of obtaining instability growth rates with good accuracy at fixed points in an accelerator. Often, it is more desirable to obtain the total instability growth with less accuracy as the beam propagates the length of the accelerator. This necessitates a simplified description of the beam dynamics. The beam breakup instability and most other $m = 1$ modes take the form at small amplitudes of rigid transverse displacements of the beam. Consequently, the beam can be represented as a string of rigid disks moving forward at a specified velocity but free to move sideways. Interaction with cavity modes and other sources of instability likewise can be represented simply by lumped parameter models. Self-fields are treated in the long wavelength approximation.

The beam centroid equation of motion is

$$\frac{d}{dt}\gamma\frac{d}{dt}\xi = i\frac{d}{dt}\omega_c\xi - \frac{2\nu}{\gamma^2 R^2}\xi + F \tag{17}$$

where $\xi = X_1 - iY_1$ measures small transverse displacements. The first term on the right side of Eq. (17) represents the magnetic guide field. The second term represents the net image force, electric less magnetic, for a cylindrical drift tube of radius R. The final term includes forces from induction modules, etc. Note that γ increases as the beam accelerates.

The oscillatory force on the beam due to $m = 1$ cavity modes giving rise to the beam breakup instability is given by[74]

$$\frac{d^2}{dt}F - \frac{\omega_0}{Q}\frac{d}{dt}F - \omega_0^2 F = \nu\omega_0^3\frac{Z_\perp}{Q} \tag{18}$$

A separate equation is required for each induction gap, and the force is applied impulsively there. $Z_\perp$ is the coupling impedance, Q the mode quality factor, and ω_0 the mode frequency. The image displacement instability arises from interruption of beam image currents at the acceleration gaps.[75]

$$F = 2\nu\frac{l}{R^2}\xi \tag{19}$$

For narrow gaps, l is the gap width. Otherwise, l must be computed numerically and is less than the gap width.[13] Finally, finite wall conductivity introduces a phase lag between image charges and currents, resulting in a distributed force,[76]

$$F = \frac{8g}{R^3}\int_0^t \frac{\partial\nu\xi}{\partial t'}\left(\frac{t-t'}{\pi\sigma}\right)^{1/2} dt' \tag{20}$$

derived in the paraxial approximation. σ is the wall conductivity, and g is a geometrical factor of order unity. Evaluating the integral is relatively time-consuming.

Codes employing these models were used to design the ATA[77] and RADLAC[11] accelerators. Figure 10 is the predicted amplification of the beam breakup instability for a 5 kA, 20 MeV, 19 module accelerator design, obtained using the BALTIC code.[78] Note that the instability wave packet starts at the beam head and slowly convects back. Growth becomes exponential only late

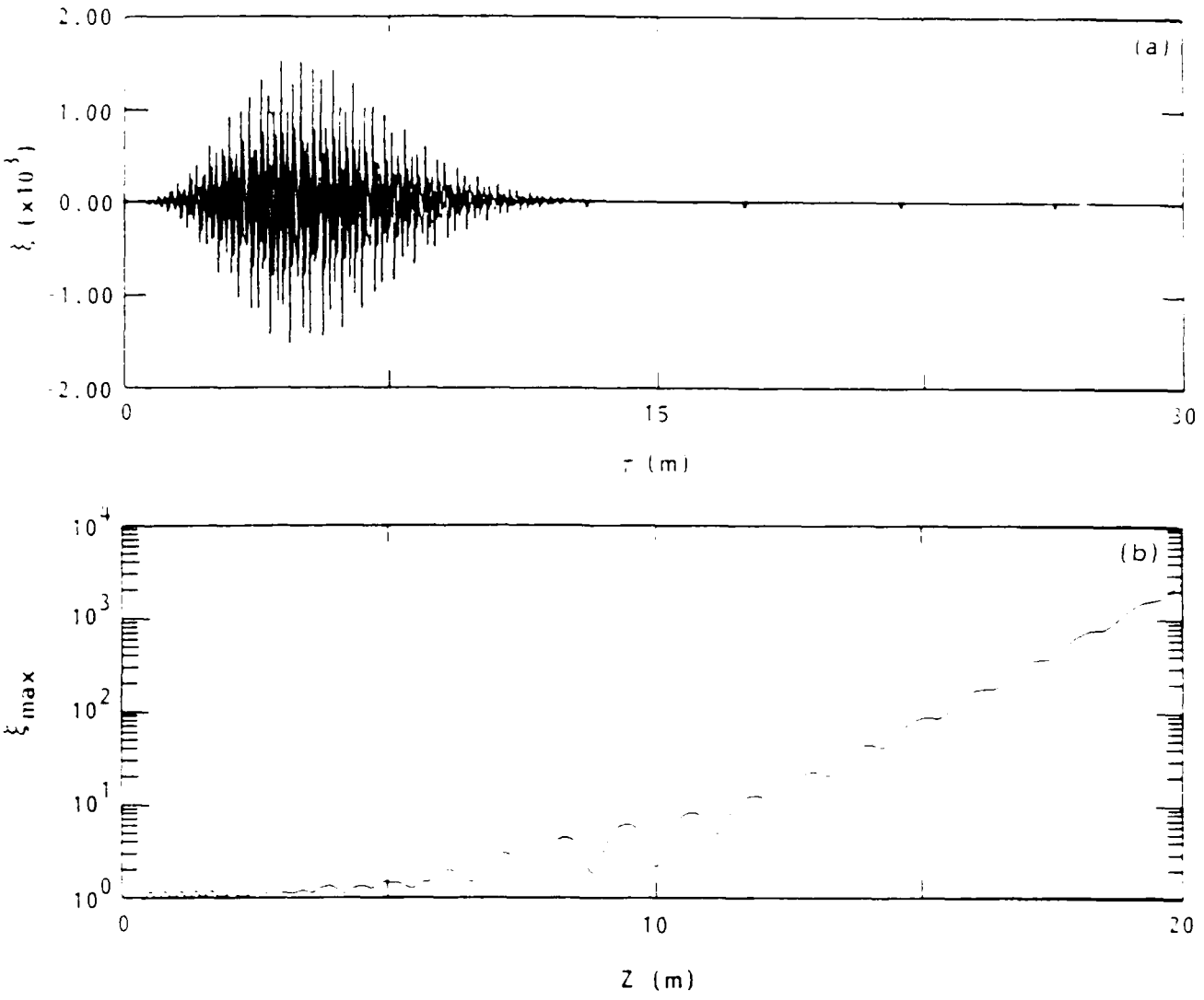

FIG. 10. Beam breakup instability (a) temporal growth into the 20 nsec pulse and (b) peak spatial growth along the 19 m accelerator. Beam voltage increases from 1 to 20 MeV; current is 5 kA. Each of 19 acceleration gaps has $Z_{\perp} = 10\ \Omega$ and $Q = 10$.

in time. This calculation required nearly a minute on a CRAY-1 computer. The code would be much faster with the resistive wall force, Eq. (20), omitted.

D. Multi-Component Beam Centroid Codes

To the extent that focusing forces on the beam particles (including self-forces) are not linear with radius, particle oscillation frequencies are a function of amplitude. Phase-mix damping of transverse instabilities due to the spread in particle oscillation frequencies can be modeled within the context of beam centroid codes by treating each beam slice as a modest number of interpenetrating rigid disks. Disks are assigned effective masses and charges corresponding to the frequency at which each oscillates and to the portion of the beam each represents, respectively.[79]

Multi-component beam centroid codes are used to simulate electron beam hose instabilities in IFT channels[80] and in air. In the latter context they are described at length in the chapter by W. Fawley.

IV. NONLINEAR PIC COMPUTATIONS

A. PIC Code Fundamentals

PIC codes determine the time evolution of complex beams and plasmas by computing the dynamics of many thousands of representative particles (electrons and/or ions) moving in electromagnetic fields externally applied or produced by the beams and plasmas themselves. Thus, PIC codes provide the most fundamental and detailed representation possible of plasma problems. In effect, they solve the Vlasov equation. Of course, this precision comes at the cost of substantial computer requirements, and for this reason PIC codes should be employed only when simpler numerical or analytical techniques described previously are inadequate.

The electromagnetic fields are defined on a regular mesh in one, two, or three dimensions, depending on the symmetry of the problem to be solved. The mesh can be in rectangular, cylindrical, or other desired geometry. At each time step, new electric and magnetic fields are computed by advancing the finite difference approximations to Maxwell's equations,

$$\frac{\partial E}{\partial t} = \nabla \times B - 4\pi J \tag{21}$$

$$\frac{\partial B}{\partial t} = -\nabla \times E \tag{22}$$

using currents (J) determined from the plasma particle motion on the previous time step. Alternatively, equations for the scalar and vector potentials can be solved. Boundary conditions are required to define spatial derivatives at the mesh edges. Wave reflecting (i.e., metallic) or periodic boundary conditions are common choices. More complicated boundaries allow electromagnetic waves to be launched into the computational region or to leave it, as described in the next subsection.

Particle momenta ($P = \gamma V$), positions (X), and energy (γ) are then advanced using the relativistic equations of motion with the newly computed fields.

$$\dot{P} = E + V \times B \tag{23}$$

$$\dot{X} = V \tag{24}$$

$$\gamma = \left(p^2 + 1\right)^{1/2} \tag{25}$$

(Replace γ by 1 for nonrelativistic problems.) The fields appearing in Eq. (23) are those at the particle location, obtained from the fields at nearby mesh points by (typically, linear) interpolation. When a particle leaves the computational region, it is destroyed or it is returned to the mesh by some prescribed procedure (e.g. reflected). By the same token, particles can be injected from boundaries, a feature particularly useful in particle beam simulations. After a particle's new position and momenta have been determined, its contribution to the plasma currents is obtained by interpolating $V = P/\gamma$ to nearby mesh points.

This cycle of advancing fields based on particle currents and then advancing particles based on the new fields is repeated hundreds of times in a typical simulation. The time step is set by the smallest time scale in the calculation, which may be the plasma oscillation period, the electron cyclotron period, or the Courant time (of order the time for a light wave to cross a cell in the mesh). Progress has been made in the last few years at surmounting the Courant limit, which is numerical rather than physical in character.[81] Cell dimensions must be small compared to spatial scales of interest.

PIC code running times and memory requirements are highly problem dependent. CPU times on a CRAY-1 computer typically range between 15 minutes and 4 hours, although 20 hour runs are not unheard of. Corresponding central memory needs vary between $2 \cdot 10^5$ and $4 \cdot 10^6$ words. At least two fast, large capacity disks or their equivalent also are needed. Historically, the physics problems attempted with PIC codes have expanded to consume the maximum resources available in each generation of computers.

PIC codes usually have extensive graphics output capabilities and operating-system interfaces. Advances in PIC technique are described in several books[82,83] as well as in the chapters here by A. Langdon and A. Mankowsky.

B. Standard PIC Codes

Most any multidimensional PIC code treating both electric and magnetic fields can, with minor modifications, be applied to beam transport. Beam simulations typically are performed in cylindrical geometry. Relativistic particle dynamics, if required and not already available, are easy to implement. Efficiency is an important consideration; beam simulations tend to be lengthy.

Boundary conditions properly modeling the often complex accelerator structures are particularly important. Figure 11, for instance, is taken from an IVORY code simulation of an image

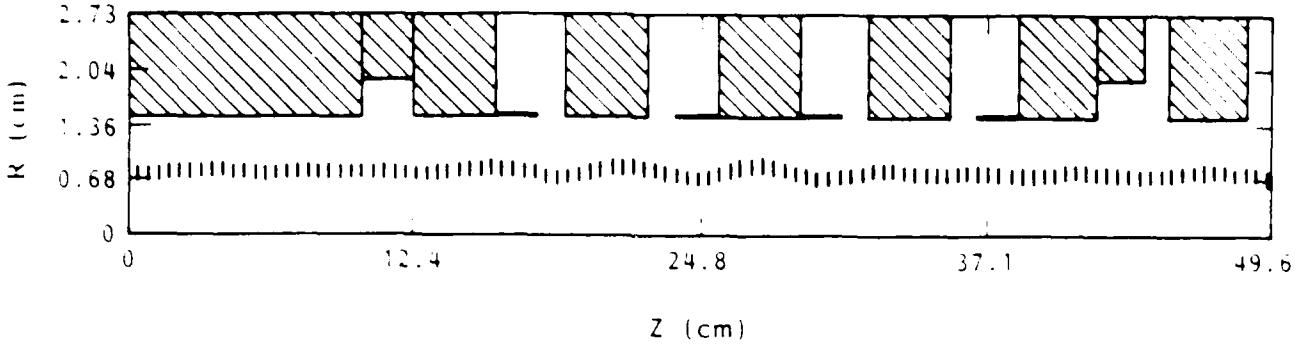

FIG. 11. Axisymmetric drift tube geometry from IVORY simulation of image displacement instability with 23 kA, 2 MeV, annular electron beam in a 10 kG guide field. Beam dynamics are nonaxisymmetric.

displacement instability experiment.[13] Shaded regions are metal disks; thick horizontal lines projecting from the disks are metal foils. Conductors are introduced on the computational mesh simply by setting tangential electric fields to zero on their boundaries. (The other field components need not be adjusted on a properly staggered mesh.) A tightly spaced helical coil can be specified by setting the field component along the winding to zero while leaving the other components alone.[84] Specifically, for a helix of pitch angle ψ, set $E_\theta \cos\psi + E_z \sin\psi = 0$ without modifying $E_\theta \sin\psi - E_z \cos\psi$. Dielectrics are treated by multiplying E in Eq. (21) by the dielectric constant ϵ. Similarly, bulk resistivity is included by adding the term σE to the left side of Eq. (21). In so doing, one must be careful not to exceed the Courant limit by allowing $\sigma\Delta t$ to become large, unless integrating factors are used.

If the simulation mesh is not large enough to accommodate the entire accelerator, then computational boundaries through which electromagnetic waves are able to pass without nonphysical reflections are essential. The standard wave-transmitting boundary condition is

$$\frac{\partial E}{\partial t} - v\frac{\partial E}{\partial x} = 2\frac{\partial E_0}{\partial t} \tag{26}$$

where E is the tangential electric field at the boundary and x is the normal coordinate, pointing inward. Any electromagnetic wave approaching the boundary with normal phase velocity v leaves the mesh without reflection, as can be verified by substituting arbitrary $E(t - x/v)$ into Eq. (26). Equation (26) also launches waves $E_0(t - x/v)$ into the computational mesh, if desired. When the primary source of electromagnetic waves is short wavelength beam fluctuations, setting v to the beam velocity minimizes spurious noise.

If waves with a spread in phase velocities strike the boundary, at least some of them are reflected. The reflected wave relative amplitude is $(v^* - v)/(v^* + v)$, where v^* is the wave phase velocity normal to the boundary. A more general boundary condition able to transmit waves at essentially all phase velocities was developed for laser-plasma interaction studies.[85] It is relatively

complex and will not be discussed here. A second alternative for wave absorption is a thick, graded resistance placed at the boundary, although a large portion of the computational mesh can be lost in this way.

An example of multidimensional simulations of accelerators is a recent instability study for high current modified betatrons, performed with the IVORY code.[86] IVORY is a three-dimensional, relativistic, electromagnetic PIC code in which fields are Fourier decomposed in the azimuthal direction rather than finite-differenced.[87] This approach is particularly efficient for problems which are approximately but not exactly axisymmetric, such as transverse oscillations on an axisymmetric beam or toroidal oscillations on an electron ring. Applied to the modified betatron, IPROP can follow instabilities in the recirculating beam for 100 m in a few hours of CRAY-1 computer time. A typical negative mass instability result is shown in Fig. 3.

The application of PIC codes to ion beam equilibrium and stability is discussed in the chapter by W. Herrmannsfeldt. Typically, a two-dimensional code is used to follow the transverse dynamics of a single beam slice as it travels the length of the accelerator.

C. Darwin Model PIC Codes

As noted in Sec. IV. A. , the time step in electromagnetic PIC codes is limited by the Courant condition. This limitation can be circumvented by implicit methods, some of which are described in the chapter by A. Langdon. Alternatively, electromagnetic waves can be eliminated entirely, if they are not necessary to the problem to be solved. Electrostatic calculations are entirely adequate for many ion beam calculations, for instance. The Darwin model can be applied efficiently, when inductive effects are important but wave effects are not.

Darwin's approximation to Maxwell's equations is derived formally by expanding the particle-field interaction Lagrangian in powers of V/c, where V is the particle velocity, and retaining terms through second order. The field equations following from the approximate Lagrangian can be written in several forms, including[88]

$$E_l = -\nabla\phi \qquad \nabla^2\phi = -4\pi\rho \tag{27}$$

$$\nabla^2 E_t = \frac{\partial}{\partial t} 4\pi J_t \tag{28}$$

$$\nabla \times B = 4\pi J + \frac{\partial}{\partial t} E_l \tag{29}$$

The subscripts "l" and "t" designate longitudinal and transverse components of the fields and currents; $\nabla \cdot E_t = 0$. Poisson's equation must be solved to obtain J_t and, of course, ϕ.[89] Nonetheless, the added cost of solving Eqs. (27)-(29) instead of Eqs. (21)-(22) is fully justified by the larger time step permitted. Numerical noise is less also.

The Darwin model is implemented in the two-dimensional DPC code, used to refine beam injection and transport systems in the ATA.[90] An interesting issue explored with DPC is acceler-

ation of electrons from the IFT channel used to guide and stabilize the primary beam. Figure 12, from this study, shows the accumulated channel electron current and energy at induction module 50.

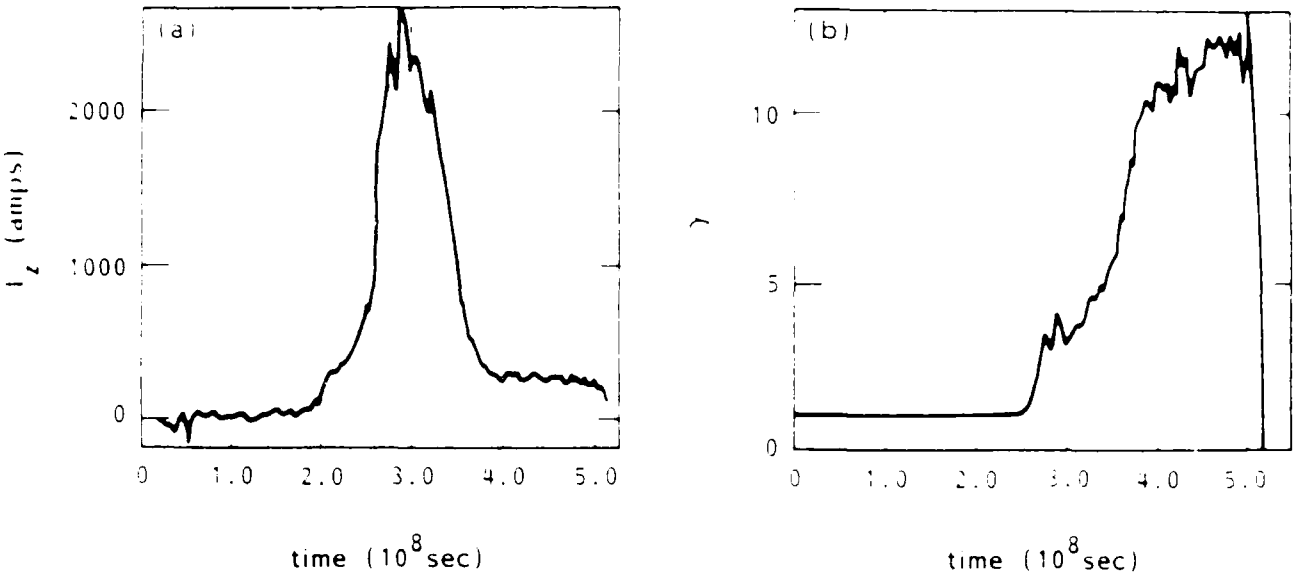

FIG. 12. Channel electron current (a) and energy (b) at ATA gap 50, predicted by the DPC code under certain circumstances.

D. PIC Codes with Co-Moving Meshes

When performing simulations of beams propagating in plasma channels, it often is convenient to use a computational mesh moving with the beam. Conceptually, this is accomplished by a Lorentz or a Galilean transformation to the beam frame. After a Lorentz transformation, PIC codes of the sort discussed above can be employed. A Galilean transformation is preferable, however, when a resistive medium is present or when the range of time scales can be compressed.

The electromagnetic field equations in a coordinate frame moving axially at velocity v are given by[91]

$$\frac{1}{2}\left[\frac{\partial}{\partial t}+(1-v)\frac{\partial}{\partial z}\right](E_r+B_\theta)+\frac{1}{2}\left[\frac{\partial}{\partial t}-(1+v)\frac{\partial}{\partial z}\right](E_r-B_\theta)+\sigma E_r=\frac{1}{r}\frac{\partial}{\partial\theta}B_z-J_r \qquad (30)$$

$$\frac{1}{2}\left[\frac{\partial}{\partial t}+(1-v)\frac{\partial}{\partial z}\right](E_r-B_\theta)-\frac{1}{2}\left[\frac{\partial}{\partial t}-(1+v)\frac{\partial}{\partial z}\right](E_r-B_\theta)=\frac{\partial}{\partial r}E_z \qquad (31)$$

$$\frac{1}{2}\left[\frac{\partial}{\partial t}+(1-v)\frac{\partial}{\partial z}\right](E_\theta+B_r)+\frac{1}{2}\left[\frac{\partial}{\partial t}-(1+v)\frac{\partial}{\partial z}\right](E_\theta-B_r)+\sigma E_\theta=-\frac{\partial}{\partial r}B_z-J_\theta \qquad (32)$$

$$\frac{1}{2}\left[\frac{\partial}{\partial t}-(1-v)\frac{\partial}{\partial z}\right](E_\theta-B_r)-\frac{1}{2}\left[\frac{\partial}{\partial t}-(1-v)\frac{\partial}{\partial t}\right](E_\theta-B_r)=\frac{1}{r}\frac{\partial}{\partial\theta}E_z \tag{33}$$

$$\frac{1}{2}\left[\frac{\partial}{\partial t}-(1-v)\frac{\partial}{\partial z}\right]E_z+\frac{1}{2}\left[\frac{\partial}{\partial t}-(1-v)\frac{\partial}{\partial z}\right]E_z+\sigma E_z=\frac{1}{r}\frac{\partial}{\partial r}rB_\theta-\frac{1}{r}\frac{\partial}{\partial\theta}B_r-J_z \tag{34}$$

$$\frac{1}{2}\left[\frac{\partial}{\partial t}+(1-v)\frac{\partial}{\partial z}\right]B_z+\frac{1}{2}\left[\frac{\partial}{\partial t}-(1-v)\frac{\partial}{\partial z}\right]B_z=-\frac{1}{r}\frac{\partial}{\partial r}rE_\theta+\frac{1}{r}\frac{\partial}{\partial\theta}E_r \tag{35}$$

Light wave axial characteristics in this frame are represented schematically in Fig. 13. Note that the forward-going characteristic crosses a constant-Z grid line before it crosses a constant-T grid line, if $\Delta z < (c-v)\Delta t$. Information at $(i-1)\Delta z$ influences the fields at $i\Delta z$ at the same time level in this case, and the Courant limit is relaxed somewhat. If, in addition, the electromagnetic coupling among radial positions at fixed Z and T is treated implicitly, the Courant limit becomes $\Delta t < \Delta z\ (c-v)$. The simulation time step typically is constrained by particle dynamics under these circumstances.

This algorithm is implemented in a version of the IVORY code known as IPROP.[31] IPROP is applied routinely to studies of relativistic electron beam propagation in low and high density plasma channels.[46,73] A lumped-parameter plasma conductivity package is available to treat weakly ionized gases in an Ohm's law approximation. Particle scattering and bremsstrahlung routines also are provided.

A significant savings in computer memory and a moderate savings in computer time can be achieved for simulations of ultrarelativistic electron beams by employing the frozen field approximation.[32] The frozen field equations are obtained from Eqs. (30)–(35) by setting $v = c$ and dropping time derivatives. Fields are solved at each particle time step by integrating the equations in Z from the head of the beam to the tail. Application of the frozen field equations to simulations of beam propagation in air is reviewed in the chapter by W. Fawley. The frozen field approximation is useful in analytical work as well, e.g., for the plasma wakefield accelerator.[8] Be aware, however, that the approximation fails for beams passing through metal foils or apertures. Like the Darwin approximation, the frozen field approximation does not treat electromagnetic radiation.[33]

V. ACKNOWLEDGMENTS

Figures 3 and 9 were provided of Dr. Thomas Hughes of Mission Research Corporation, Fig. 4 by Dr. Dushan Mitrovich of Mission Research Corporation, Fig. 5 by Dr. Lawrence Wright of Mission Research Corporation, Figs. 6 and 7 by Dr. John Freeman of Sandia National Laboratories, Fig. 11 by Dr. Mark Campbell of Mission Research Corporation, and Fig. 12 by Dr. John Boyd of Lawrence Livermore National Laboratory.

The preparation of this chapter was supported in part under a contract with the Defense Advance Research Projects Agency, monitored by the Naval Surface Weapons Center.

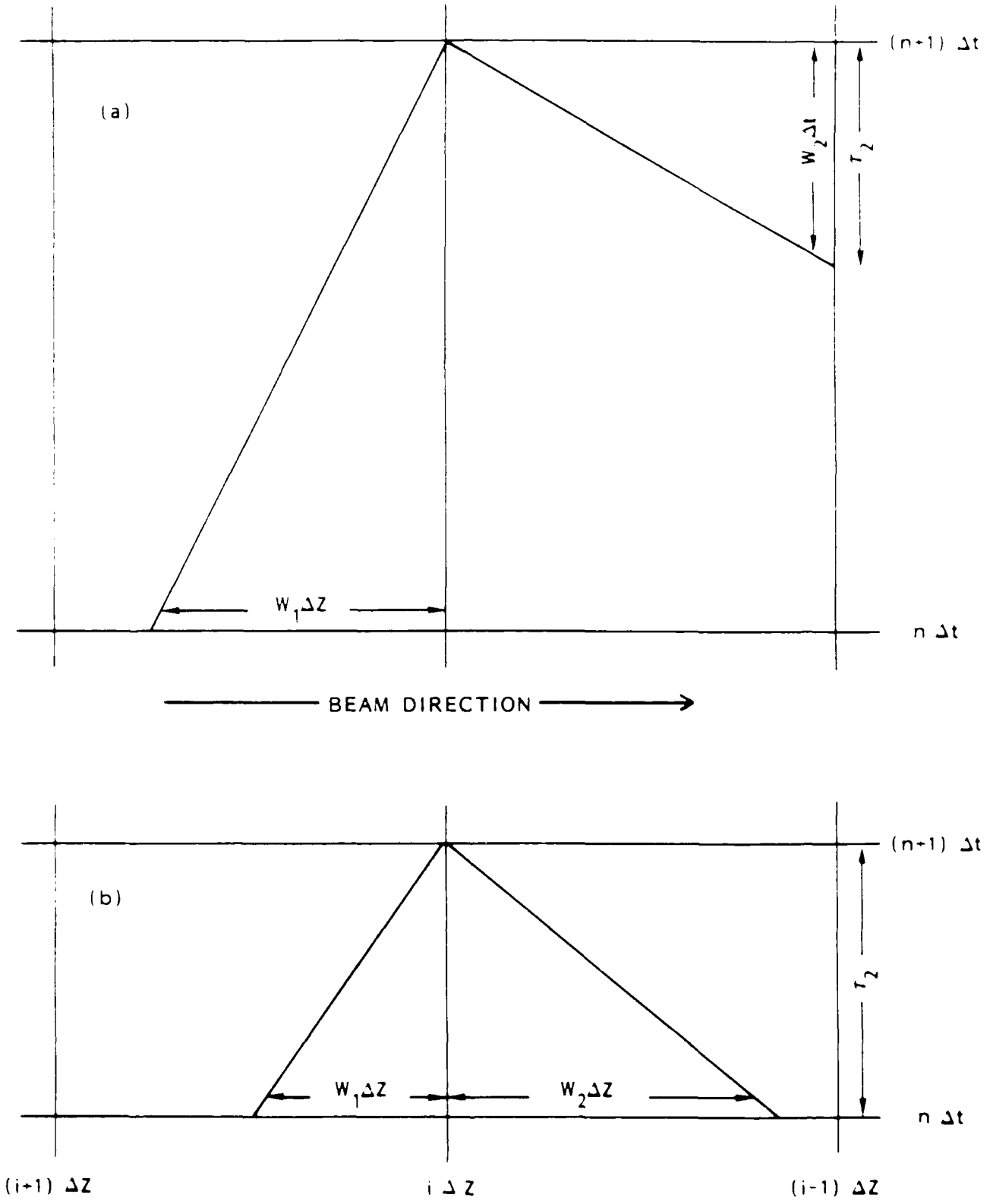

FIG. 13. Typical Z-T coordinate meshes for (a) $\Delta z < (c+v)\Delta t$ and (b) $\Delta z > (c-v)\Delta t$. Forward- and backward-going light lines and linear interpolation values W_1 and W_2 are shown.

VI. REFERENCES

[1]E. M. McMillan, ed., "Electron Ring Accelerators," UCRL-18103 (Lawrence Berkeley Laboratory, Berkeley, 1968).

[2]D. W. Kerst, Phys. Rev. 60, 47 (1941).

[3]D. W. Kerst and R. Serber, Phys. Rev. 60, 53 (1941).

[4]N. Rostoker and M. Reiser (ed.), Collective Methods of Acceleration (Harwood Academic Press, New York, 1979).

[5]C. L. Olson and U. Schumacher, Collective Ion Acceleration (Springer, New York, 1979).

[6]P. A. Channell, Laser Acceleration of Particles (American Institute of Physics, New York, 1982).

[7]H. Hora and G. H. Miley (ed.), Laser Interaction and Related Plasma Phenomena, Vol. 6 (Plenum, New York, 1984), Sec. VIII.

[8]T. Katsouleas (ed.), IEEE Trans. Plas. Sci. PS-15, 88-237 (1987).

[9]A. I. Pavlovskii, V. S. Bosamykin, V. A. Savchenko, A. P. Klement'ev, K. A. Morunov, V. S. Nikol'skii, A. I. Gerasimov, V. A. Tananakin, V. F. Basmanov, D. I. Zenkov, V. D. Selemir, and A. S. Fedotkin, Dokl. Akad. Nauk SSR 250, 1118 (1980) [Sov. Phys. Dokl. 25, 120 (1980)].

[10]D. S. Prono, IEEE Trans. Nuc. Sci. NS-32, 3144 (1985).

[11]R. B. Miller, IEEE Trans. Nuc. Sci. NS-32, 3149 (1985).

[12]R. B. Miller, J. W. Poukey, B. G. Epstein, S. L. Shope, T. C. Genoni, M. Franz, B. B. Godfrey, R. J. Adler, and A. Mondelli, IEEE Trans. Nuc. Sci. NS-28, 3343 (1981).

[13]R. Adler, M. Campbell, B. Godfrey, D. Sullivan, and T. Genoni, Part. Accel. 13, 25 (1983).

[14]V. K. Neil, L. S. Hall, and R. K. Cooper, Part. Accel. 9, 213 (1979).

[15]R. J. Briggs, D. L. Birx, G. J. Caporaso, V. K. Neil, and T. C. Genoni, Part. Accel. 18, 41 (1985).

[16]J. Poukey, B. Godfrey, T. Hughes, and M. Campbell, IEEE Trans. Nuc. Sci. NS-30, 2389 (1983).

[17]G. J. Caporaso, W. A. Barletta, and V. K. Neil, Part. Accel. 11, 71 (1980).

[18]C. W. Roberson, IEEE Trans. Nuc. Sci. NS-28, 3433 (1981).

[19]M. A. Wilson, IEEE Trans. Nuc. Sci. NS-28, 3375 (1981).

[20]A. Mondelli, D. Chernin, S. D. Putnam, L. Schlitt, and V. Bailey, Beams '86, (Osaka Univ., Osaka, 1986), p. 755.

[21]C. W. Roberson, A. Mondelli, and D. Chernin, Part. Accel. 17, 79 (1985).

[22]A. I. Pavlovskii, G. D. Kuleshov, G. V. Sklizkov, Y. A. Zysin, and A. I. Gerasimov, Dokl. Akad. Nauk SSSR 160, 68 (1965) [Sov. Phys. Dokl. 10, 30 (1967)].

[23]C. A. Kapetanakos, P. Sprangle, D. P. Chernin, S. J. Marsh, and I. Haber, Phys. Fluids 26, 1634 (1983).

[24]A. I. Pavlovskii, G. D. Kuleshov, A. I. Gerasimov, A. P. Klement'ev, V. O. Kuznetsov, V. A. Tananakin, and A. D. Tarasov, Zh. Tekh. Fiz. 47, 370 (1977) Sov. Phys. Tech. Phys. 22, 215 (1977).

[25]C. A. Kapetanakos, P. Sprangle, and S. J. Marsh, Phys. Rev. Lett. 49, 471 (1982).

[26]R. W. Landau and V. K. Neil, Phys. Fluids 9, 2412 (1966).

[27]B. B. Godfrey and T. P. Hughes, Part. Accel. 21, 173 (1987).

[28]T. P. Hughes, Beams '86 (Osaka Univ., Osaka, 1986), p. 815.

[29]T. P. Hughes and B. B. Godfrey, Phys. Fluids 29, 1698 (1986).

[30]D. Chernin and P. Sprangle, Part. Accel. 12, 101 (1982).

[31]B. B. Godfrey, B. S. Newberger, L. A. Wright, and M. M. Campbell, "IFR Transport in Recirculating Accelerators," AMRC-R-741 (Mission Research Corporation, Albuquerque, 1985).

[32]R. J. Briggs, "Suppression of Transverse Beam Breakup Modes in an Induction Accelerator by Gas Focusing," UCID-18633 (Lawrence Livermore National Laboratory, Livermore, 1980).

[33]B. Hui and Y. Y. Lau, Phys. Rev. Lett. 53, 2024 (1984).

[34]S. L. Shope, C. A. Frost, G. T. Leifeste, C. E. Crist, P. D. Kiekel, J. W. Poukey, and B. B. Godfrey, IEEE Trans. Nuc. Sci. NS-32, 3091 (1985).

[35]H. L. Buchanan, Phys. Fluids 30, 221 (1987).

[36]R. F. Schneider and J. R. Smith, Phys. Fluids 29, 3917 (1986).

[37]S. Humphries, J. Freeman, J. Greenly, G. W. Kuswa, C. W. Mendel, J. W. Poukey, and D. Woodall, "Production and Post-Acceleration of Intense Ion Beams in Magnetically Insulated Gaps," SAND79-1673 (Sandia National Laboratories, Albuquerque, 1979).

[38]A. Hyder, F. Rose, and A. Guenther (ed.), High Brightness Accelerators (Plenum, New York, 1988).

[39]E. P. Lee and R. K. Cooper, Part. Accel. 7, 83 (1976).

[40]E. P. Lee, Phys. Fluids 19, 60 (1976).

[41]E. P. Lee, "Determination of the Radius of a Self-Pinched Beam from its Energy Integral," UCID-18495 (Lawrence Livermore National Laboratory, Livermore, 1980).

[42]D. Mitrovich, "A Model for Calculating Phermex Performance," AMRC-R-661 (Mission Research Corporation, Albuquerque, 1984).

[43]G. Caporaso, private communication (1987).

[44]W. B. Herrmannsfeldt, "Electron Trajectory Program," SLAC-226 (1979).

[45]A. C. Paul, "EBQ Code—Transport of Space Charge Beams in Axially Symmetric Devices," UCID-8005 (Lawrence Berkeley Laboratory, Berkeley, 1978).

[46]B. B. Godfrey, Phys. Fluids 30, 575 (1987).

[47]R. C. Davidson, Theory of Nonneutral Plasmas (Benjamin, New York, 1974), Ch. 3.1.

[48]W. H. Bennett, Phys. Rev. 45, 890 (1934).

[49]W. H. Bennett, Phys. Rev. 98, 1584 (1955).

[50]L. A. Wright and B. B. Godfrey, "A Directory of Equilibrium Distribution Functions for Use in the Orbit Code," AMRC-R-413 (Mission Research Corporation, Albuquerque, 1982).

[51]R. J. Adler and L. A. Wright, unpublished (1983).

[52]G. J. Caporaso and A. G. Cole, IEEE Trans. Nuc. Sci. NS-30, 2618 (1983).

[53]R. J. Adler, Part. Accel. 12, 39 (1982).

[54]J. R. Freeman, "Simulations of Beam Transport in an IFR Propagation Channel," SAND86-0797 (Sandia National Laboratories, Albuquerque, 1986).

[55]T. P. Hughes and B. B. Godfrey, Phys. Fluids 27, 1531 (1984).

[56]G. Moliere, Z. Naturforsch. A3, 78 (1948).

[57]E. Keil, E. Zeitler, and W. Zinn, Z. Naturforsch. A15, 1031 (1960).

[58]I. Lerche, J. Math. Phys. 8, 1838 (1967).

[59]G. J. Caporaso, W. A. Barletta, and V. K. Neil, Part. Accel. 11, 71 and 182 (1980).

[60]J. F. Traub, Iterative Methods for the Solution of Equations (Prentice-Hall, Englewood Cliffs, 1964), Ch. 10.

[61]B. B. Godfrey, "Muller's Method Root Solver and CTSS Interface for Dispersion Relation Programs," AMRC-N-368 (Mission Research Corporation, Albuquerque, 1987).

[62]I. O. Kerner, Num. Math. 8, 290 (1966).

[63]D. Kahaner, "Zeroes of a Polynomial with Optional Error Bounds," C217 (Los Alamos National Laboratory, Los Alamos, 1979).

[64]B. B. Godfrey, IEEE Trans. Plas. Sci. PS-7, 33 (1979).

[65]R. C. Davidson, Theory of Nonneutral Plasmas (Benjamin, New York, 1974), p. 21-24.

[66]L. F. Shampine, H. A. Watts, and S. M. Davenport, SIAM Rev. 18, 376 (1976).

[67]B. B. Godfrey, "Resistive Wall Instabilities in Radial Pulseline Accelerators," AMRC-R-345 (Mission Research Corporation, Albuquerque, 1982).

[68]M. L. Sloan and W. E. Drummond, Phys. Rev. Lett. 31, 1234 (1973).

[69]P. Sprangle, A. T. Drobot, and W. M. Manheimer, Phys. Rev. Lett. 36, 1880 (1976).

[70]B. B. Godfrey and B. S. Newberger, J. Appl. Phys. 50, 45 (1979).

[71]A. Friedman, R. N. Sudan, and J. Denavit, J. Comp. Phys. 40, 1 (1981).

[72]T. P. Hughes and B. B. Godfrey, "KMRAD: A Linearized Particle Code for the Study of Resistive Instabilities," AMRC-R-364 (Mission Research Corporation, Albuquerque, 1982).

[73]T. P. Hughes and B. S. Newberger, "Electrostatic Focusing in Compact Recirculating Accelerators," AMRC-R-896 (Mission Research Corporation, Albuquerque, 1987).

[74]R. J. Adler and B. B. Godfrey, "Radial Pulseline Electron Accelerator Study," AMRC-R-368 (Mission Research Corporation, Albuquerque, 1982).

[75]V. K. Neil, "The Image Displacement Effect in Linear Induction Accelerators," UCID-17976 (Lawrence Livermore National Laboratory, Livermore, 1978).

[76]S. Bodner, V. K. Neil, and L. Smith, Part. Accel. 1, 327 (1970).

[77]G. J. Caporaso, A. G. Cole, and K. W. Struve, "Beam Breakup Instability Experiments on the Experimental Test Accelerator and Predictions for the Advanced Test Accelerator," UCRL-88262 (Lawrence Livermore National Laboratory, Livermore, 1983).

[78]B. B. Godfrey, unpublished.

[79]E. P. Lee, Phys. Fluids 21, 1327 (1978).

[80]G. J. Caporaso, A. G. Cole, and E. J. Lauer, "IFR Hose Theory," UCRL-92874 (Lawrence Livermore National Laboratory, Livermore, 1985).

[81]B. I. Cohen, ed., Multiple Time Scales (Academic Press, Orlando, 1985).

[82]B. Adler, S. Fernbach, and M. Rotenberg, eds., Meth. Comp. Phys., Vol. 9 (1972).

[83]C. K. Birdsall and A. B. Langdon, Plasma Physics via Computer Simulation (McGraw-Hill, New York, 1985.

[84]B. B. Godfrey, R. J. Faehl, B. S. Newberger, W. R. Shanahan, and L. E. Thode, Beams '77 (Cornell Univ., Ithaca, 1977), Vol. II, p. 541.

[85]E. L. Lindman, J. Comp. Phys. 18, 66 (1975).

[86]T. P. Hughes and B. B. Godfrey, "Modified Betatron Accelerator Study," AMRC-R-655 (Mission Research Corporation, Albuquerque, 1984).

[87]M. M. Campbell and B. B. Godfrey, "IVORY User's Manual," AMRC-R-454 (Mission Research Corporation, Albuquerque, 1983).

[88]C. W. Neilson and H. R. Lewis, Meth. Comp. Phys. 16, 367 (1976).

[89]J. K. Boyd, "Numerical Determination of Injector Quality for High Beam Quality," UCRL-93456 (Lawrence Livermore National Laboratory, Livermore, 1985).

[90]J. K. Boyd, "Simulation of an ATA-E-Beam Formed from a Laser-Generated Plasma," UCRL-92844 (Lawrence Livermore National Laboratory, Livermore, 1985).

[91]B. B. Godfrey, "The IPROP Three-dimensional Beam Propagation Code," AMRC-R-966 (Mission Research Corporation, Albuquerque, 1987).

[92]E. P. Lee, "The New Field Equations," UCID-17286 (Lawrence Livermore National Laboratory, Livermore, 1976).

[93]J. K. Boyd, E. P. Lee, and S. S. Yu, "Aspects of Three Field Approximations: Darwin, Frozen, Empuise," UCID-20453 (Lawrence Livermore National Laboratory, Livermore, 1985).

END

DATE

FILMED

6-88

DTIC